Fully relativistic configuration-interaction calculations on the vibrational and electronic structure of the $2p^{-1} \rightarrow 3p(\pi,\sigma)^{-2}$ normal Auger-electron spectrum of HCl

K. Ellingsen,[1] T. Matila,[2] T. Saue,[1] H. Aksela,[2] and O. Gropen[1]
[1]*Department of Chemistry, Faculty of Science, University of Tromsø, N-9037 Tromsø, Norway*
[2]*Department of Physical Sciences, P.O. Box 3000 University of Oulu, FIN-90014 Oulu, Finland*
(Received 16 February 2000; published 11 August 2000)

Fully relativistic configuration-interaction calculations, based on the Dirac-Coulomb Hamiltonian, were performed on the ground state of HCl, the Cl $2p$–ionized HCl^+, and the $3p(\pi,\sigma)^{-2}$ states of HCl^{2+}. Calculated ionization energies and bond lengths were found to be in good agreement with recent experimental results and previous calculations. The potential-energy curves were used in calculating vibrational profiles of selected Auger transitions. Nonadiabatic effects in the spin-orbit-induced avoided level crossing were investigated using diabatic electronic basis sets.

PACS number(s): 31.10.+z, 32.80.Hd, 31.30.Jv, 33.70.−w

I. INTRODUCTION

Relativistic effects are normally not considered to be of importance for molecules containing light elements ($Z \leqslant 40$). However, for processes or properties probing the electron density near nuclei this may no longer be correct, as was, for instance demonstrated by our results from fully relativistic configuration-interaction calculations on Cl $2p$–ionized HCl^+ [1]. It was shown that core-valence correlation treatment and a two-electron operator based on relativistic theory [the Coulomb operator corrected by the Gaunt (Breit) operator] were required to obtain reliable binding energies with correct spin-orbit and molecular field splittings [1]. In this paper we present results of similar calculations on HCl^{2+}. Even for this valence doubly ionized species, relativistic effects need to be considered as spin-orbit coupling induces avoided crossings. We combine our results to study the $2p^{-1} \rightarrow 3p(\pi,\sigma)^{-2}$ normal Auger-electron spectrum (AES) of HCl. In a recent study of the AES of HCl, spin-orbit interaction was included as a perturbation in the nonrelativistic treatment of the $2p$-ionized state [2]. In the final state of Auger decay, relativistic effects were, however, fully disregarded. In our work on the Br $3d$–ionized HBr^+ and valence double ionized HBr^{2+} states [3], we observed avoided level crossings caused by spin-orbit interaction in HBr^{2+} leading to a change in intensity between the various components of the vibrational bands and situations where transitions to vibrational and continuum states are present simultaneously in the AES. Lifetime vibrational interference was found to be of great importance. In this paper we will study these effects on HCl^{2+}, although expected to be less prominent. We compare our results to those reported in several experimental works [4–6] as well as by Banichevich *et al.* [7], who performed nonrelativistic multireference (MR) configuration-interaction calculations employing the Breit-Pauli operator on the wave functions to investigate spin-orbit effects.

II. ADIABATIC POTENTIAL-ENERGY CURVES, VIBRATIONAL ENERGIES, AND WAVE FUNCTIONS

A. Computational details

All calculations were performed using the MOLFDIR [8] program package. The nuclei were represented by a finite-nucleus model; i.e., by a Gaussian charge distribution [9] with exponent 0.8959×10^9 for Cl. The calculations were carried out in C_{4v} double-group symmetry, because the full symmetry of the problem, $C_{\infty v}$, cannot be exploited by the MOLFDIR package. The two-electron interaction was represented by treating the Coulomb operator variationally. Test calculations with the Gaunt operator were performed.

Overlap selection was employed to converge the $2p$-ionized states and Mulliken population analysis was used to monitor convergence to the desired state.

DHF spinors for the $3p(\pi,\sigma)^{-2}$ states were generated averaging four electrons over the $3p(\pi,\sigma)$ spinors. The different states arising from the open-shell manifold were projected out through a complete open-shell configuration-interaction (COSCI) calculation.

Correlation was handled by restricted active space configuration interaction (RASCI) calculations. Two different types of calculations were performed, CI_{valence} (CI_v) and $CI_{\text{valence+core}}$ (CI_{v+c}). In the CI_v calculations, electrons in the $3s(\sigma)$ and $3p(\pi,\sigma)$ spinors were correlated. In the CI_{v+c} calculations, electrons in the $2p$ spinors were correlated as well. The RAS spaces were constructed as shown in Table I. All excitations from the RAS1 to the RAS2 subspaces, all possible excitations within the RAS2 subspace, and single and double excitations from RAS1 to RAS3 were allowed giving a multireference description for the $3p(\pi,\sigma)^{-2}$ states in both types of CI calculations and for the $2p^{-1}$ states in the CI_{v+c} calculations. All spinors with energy above 5 a.u. were deleted. Several roots were taken out in each symmetry.

For the large components of chlorine, a $(14s10p7d1f)$ relativistically optimized, primitive basis set generally contracted to $[3s+4,4p+4,7,1]$ and for the large components of hydrogen a $(6s3p1d)$ primitive basis with exponents from Dunning [10] generally contracted to $[3s+3,3,1]$ were applied. Basis sets for the small components of chlorine and hydrogen were generated by the atomic balance relation [11]. The basis sets are described in detail in [1].

Spectroscopic constants for the ground state and the $2p$-ionized states were obtained by fitting the potential-energy curves around the equilibrium distance to polynomials (of different orders). For the $3p(\pi,\sigma)^{-2}$ states of HCl^{2+},

TABLE I. RAS spaces used in CI_v and CI_{v+c} calculations.

State	CI_v			CI_{v+c}		
	RAS1	RAS2	RAS3	RAS1	RAS2	RAS3
Ground state	$3s(\sigma),3p(\pi,\sigma)$		virtual spinors	$2p,3s(\sigma),3p(\pi,\sigma)$		virtual spinors
$2p^{-1}$	$2p$ hole spinor [a]	$3s(\sigma),3p(\pi,\sigma)$	virtual spinors	occ. $2p$ spinors, $3s(\sigma),3p(\pi,\sigma)$	$2p$ hole spinors	virtual spinors
$3p(\pi,\sigma)^{-2}$	$3s(\sigma)$	$3p(\pi,\sigma)$	virtual spinors	$2p,3s(\sigma)$	$3p(\pi,\sigma)$	virtual spinors

[a]The unoccupied Kramers partner of the open $2p$ spinor pair is deleted.

the calculated points of the potential curves were first subjected to a spline fit. Vibrational energies and wave functions were thereafter calculated by numerical integration of the nuclear Schrödinger equation.

Only the quantum numbers ω and Ω are feasible within a relativistic scheme. However, while the HCl core spinors are best described in terms of $\omega\omega$ coupling, the valence spinors display $\lambda\sigma$ coupling [1]. We have therefore chosen the nonrelativistic $\Lambda\Sigma$ notation to characterize the $3p(\pi,\sigma)^{-2}$ states.

B. The ground state and the Cl $2p$−ionized states

Results on the ground state and the Cl $2p$−ionized states were previously discussed thoroughly [1]. We have expanded our calculations to obtain bond lengths and vibrational constants both on the DHF and the correlated level. These results are presented in Tables II and III.

For the ground state we obtain a bond lenght of 1.280 Å at the CI_{v+c} level, well in line with the experimental value of 1.2746 [12] and the fully relativistic calculations of Visscher *et al.* [13]. The harmonic vibrational constant of 3013 cm^{-1} is in accord with the experimental result of 2991 cm^{-1} [12] as well as the calculated results of Visscher *et al.* [13].

The bond lengths of the three core-ionized states deviate only slightly from each other, being 1.30 Å at the CI_v level. The inclusion of core-valence correlation has virtually no effect on the bond lengths. The bond lengths at the correlated level are in correspondence with the experimental result of 1.297 Å for $2p^{-1}_{1/2,1/2}$ by Püttner *et al.* [14] and with an earlier estimate of about 1.30 Å in Ref. [4].

The harmonic vibrational constants of the three Cl $2p$−ionized states differ only slightly, confirming the similar and parallel shape of the potential curves of these states. The differences between the DHF values and correlated values are neglible. At the CI_{v+c} level we obtained 2728 cm^{-1}, 2747 cm^{-1}, and 2719 cm^{-1} for the $2p^{-1}_{1/2}$, $2p^{-1}_{3/2,1/2}$, and $2p^{-1}_{3/2,3/2}$ states, respectively. These values agree with an experimentally derived value of 2879(40) cm^{-1} [14].

C. The valence ionized states of HCl^{2+}

In $\Lambda\Sigma$ coupling the $3p(\pi,\sigma)^{-2}$ states of HCl^{2+} can be be divided into three groups. The σ^{-2} state ($^1\Sigma^+$) has two holes in the bonding $3p\sigma$ orbital and is expected to be strongly dissociative. On the other hand, the π^{-2} states ($^3\Sigma^-$, $^1\Delta$, and $^1\Sigma^+$) with holes in the nonbonding $3p\pi$ orbitals are expected to be bound. The mixed $\sigma^{-1}\pi^{-1}$ states ($^3\Pi$ and $^1\Pi$) are dissociative. Spin-orbit coupling is perturbing this picture. In particular, the spin-orbit interaction between the bonding $^1\Sigma^+_{0-}$ and the dissociative $^3\Pi_{0-}$ leads to an avoided crossing. Another avoided crossing created by the same mechanism is observed between the bonding $^1\Delta_2$ and the dissociative $^3\Pi_2$. Fully relativistic $(\pi,\sigma)^{-2}$ MRCI potential curves are presented in Fig. 1 with the exception of the strongly repulsive σ^{-2} ($^1\Sigma^+_{0-}$), which is lying much higher in energy. This potential curve behaves at longer distances as a Coulomb interaction between two charges, i.e., as $1/R$, R being the internuclear distance. This is illustrated in Fig. 2, where we have plotted the σ^{-2} ($^1\Sigma^+_{0-}$) potential

TABLE II. Bond lengths in Å for the Cl $2p$−ionized and the doubly valence ionized states in adiabatic approximation. CI calculations in which the Davidson correction is included are referred to as CI+Q.

	DHF	$CI_v(+Q)$	$CI_{v+c}(+Q)$	Expt.	Other Refs.
Ground state	1.264	1.266(1.267)	1.280(1.285)	1.2746 [12]	1.267, [a] 1.273(1.278) [b] [13]
$2p^{-1}_{1/2}$	1.286	1.301(1.306)	1.302(1.308)	1.297 [14], 1.30 [4]	
$2p^{-1}_{3/2,1/2}$	1.288	1.304(1.309)	1.304(1.310)		
$2p^{-1}_{3/2,3/2}$	1.284	1.299(1.303)	1.300(1.305)		
$3p\pi^{-2}$ ($^3\Sigma^-_{0+,1}$)	1.430	1.450		1.39 [5], 1.44 [4]	1.46 [c] [7]
$3p\pi^{-2}$ ($^1\Delta_2$)	1.433	1.449		1.44 [5], 1.48 [4]	1.46 [c] [7]
$3p\pi^{-2}$ ($^1\Sigma^+_{0-}$)	diss.	1.467		1.49 [4]	1.47 [c] [7]
$3p\pi^{-2}$ ($^3\Pi_2$)	1.905	2.015			
$3p\pi^{-2}$ ($^3\Pi_{0-}$)	1.486	1.590			

[a]DHF calculation.

[b]Fully relativistic CISD calculation, Davidson-corrected value in parentheses.

[c]Nonrelativistic MRCI calculation.

TABLE III. Vibrational constants in cm^{-1} for the Cl $2p$–ionized and the doubly valence ionized states.

			$\omega, x\hbar\omega$		
	DHF	$CI_v(+Q)$	$CI_{v+c}(+Q)$	Expt.	Other Refs.
Ground state	3135	3121(3118)	3013(2953)	2991 [12]	3132, [a] 3046 (2995) [b] [13]
$2p_{1/2}^{-1}$	2680	2717 (2717)	2728 (2729)	2879(40) [14]	
$2p_{3/2,1/2}^{-1}$	2692	2730 (2728)	2747 (2741)		
$2p_{3/2,3/2}^{-1}$	2666	2704 (2705)	2719 (2721)		
$3p\pi^{-2}$ ($^3\Sigma_{0+}^-$)	1892, 235	1754, 217		1566,81 [5], [d]1791,123 [4] [d]	1758, 129 [7] [c]
$3p\pi^{-2}$ ($^3\Sigma_1^-$)	1870, 231	1767, 219			
$3p\pi^{-2}$ ($^1\Delta_2$)		1863, 149 [e]		1508,60 [5], [d] 1589,101 [4] [d]	1797, 136 [7] [c]

[a]DHF calculation.
[b]Fully relativistic CISD calculation, Davidson-corrected value in parentheses.
[c]Nonrelativistic MRCI calculation.
[d]Refitted using vibrational states $\nu=0-3$.
[e]MRCI calculation using vibrational states $\nu=0-2$ in approximate diabatic basis.

curve along with a $1/R$ curve obtained using the calculated energy in the dissociation limit $[H^+ + Cl^+(^1S_0)]$ as an asymptote.

Vibrational energies and wave functions were obtained by solving the nuclear Schrödinger equation for each electronic state separately. This approach is not valid for the adiabatic states involved in avoided crossings due to the breakdown of the Born-Oppenheimer approximation. Vibrational functions for these states were therefore generated after explicit construction of a diabatic basis. For the avoided crossing between $^1\Sigma_{0-}^+$ and $^3\Pi_{0-}$ we proceeded as described in [3]. We note that the $0+$ component of the $^3\Pi$ state does not interact with other states through spin-orbit coupling and thereby represents the unperturbed $0-$ component. This allows the extraction of the potential curve for the unperturbed $^1\Sigma_{0-}^+$ as well as the spin-orbit coupling elements at each internuclear distance. The unperturbed states are smooth functions of the internuclear distance and form a diabatic electronic basis. The nuclear Schrödinger equation can now be solved for each of the two diabatic states when the spin-orbit coupling is neglected. Finally, the ensemble of diabatic vibronic states was used as a basis for the variational solution of the full molecular Hamiltonian (rotation neglected), that is, without the Born-Oppenheimer approximation. This procedure allowed us to analyze the effect of spin-orbit coupling on the vibronic spectra. A diabatic basis was approximated for the $^1\Delta_2$ and $^3\Pi_2$ states using a vertically shifted $^3\Pi_1$ curve to represent the unperturbed $^3\Pi_2$ state.

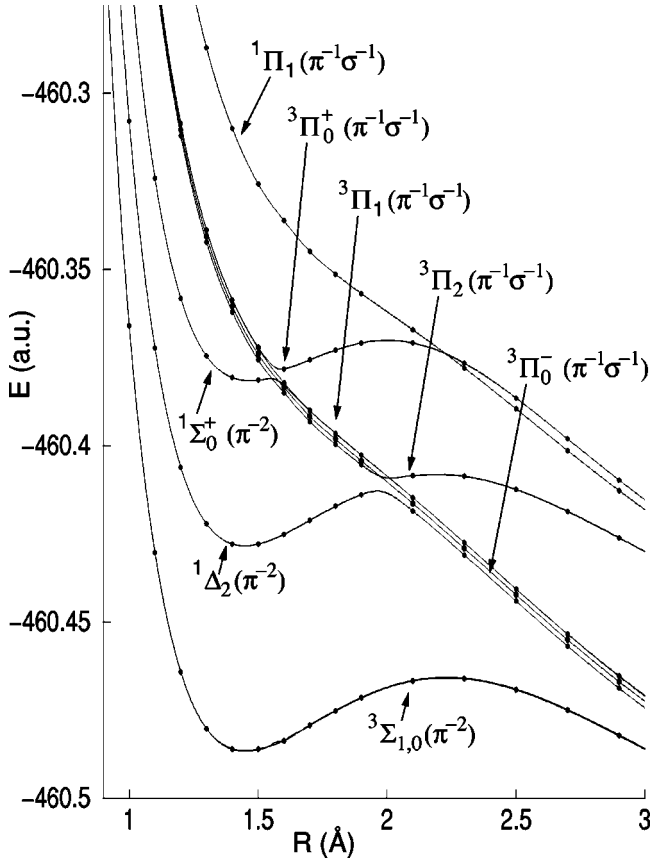

FIG. 1. Potential-energy curves for the $3p\pi^{-2}$ and $3p\sigma^{-1}3p\pi^{-1}$ states of HCl^{2+} calculated at the CI_v level.

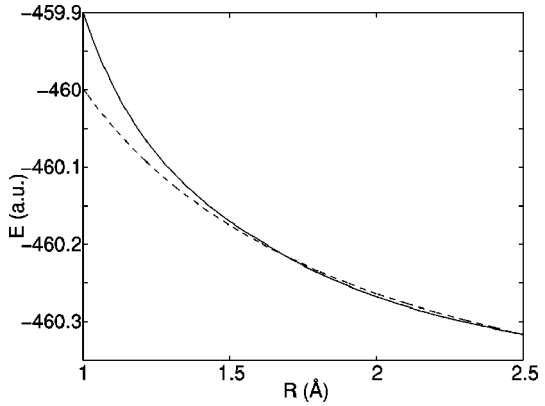

FIG. 2. CI_v potential energy for the repulsive $3p\sigma^{-2}$ state $^1\Sigma_{0-}^+$ (solid line) plotted together with a curve representing a Couloumbic interaction between two charges obtained using the calculated dissociation energy as an asymptote (dashed line).

TABLE IV. Experimental [5] and calculated adiabatic binding energies of HCl^{2+}. All energies are in eV.

State	ν	Expt. [5]	DHF	CI_v	Nonrel. [7]
$3p\pi^{-2}(^3\Sigma_1^-)$	0	35.59	33.310	35.948	35.60
$3p\pi^{-2}(^3\Sigma_1^-)$	1	35.76	33.505	36.140	35.78
$3p\pi^{-2}(^3\Sigma_1^-)$	2	35.92	33.664	36.304	35.93
$3p\pi^{-2}(^1\Delta_2)$	0	37.08	35.102	37.532	37.16
$3p\pi^{-2}(^1\Delta_2)$	1	37.25	35.289	37.721	37.34
$3p\sigma^{-1}3\pi^{-1}(^3\Pi_{0-})$	0		36.702	38.919	39.63

Bond lengths and vibrational constants are given in Tables II and III. The splittings of the vibrational levels can be deduced from Table IV.

The $^3\Sigma_{0+}^-$ state is well separated from the other states and shows no spin-orbit effects, apart from the small fine-structure splitting (3 meV) of the $\Omega=0$ and $\Omega=1$ components. The potential curves of the two fine-structure components are perfectly parallel and we find the minima at 1.430 Å on the DHF level augmenting to 1.450 Å on the CI level. The potential well possesses three vibrational levels split by 192 meV and 356 meV relative to the $\nu=0$ state on the CI_v levels in excellent agreement with the corresponding experimental values [4,5]. Five vibrational levels were found in experimental studies [4,5]. More recent experiments [6] indicate, however, that Auger transitions to the uppermost vibrational levels appear as a broad band corresponding to continuum transitions. Nonrelativistic MRCI results show three vibrational levels split by 180 and 330 meV, respectively [7].

The $^1\Delta_2$ state is bound with a minimum at 1.449 Å on the CI level. In the adiabatic basis the potential well supports two vibrational levels. Using the approximate diabatic basis, an additional $\nu=2$ vibrational level is clearly visible in accordance with the result of three levels found in nonrelativistic calculations [7]. From the calculations of both the Auger transitions and the direct double ionization, we found an additional small hump in the continuum band which replicates the vibrational level $\nu=3$ consistently with experimental findings [4,5]. The splitting between $\nu=0$ and $\nu=1$ states is 189 meV at the adiabatic CI_v level, changing slightly to 194 meV when the approximate diabatic basis was used. The splitting between $\nu=0$ and $\nu=2$ levels was found to be 351 meV and the difference between the ''$\nu=3$'' hump (the center of 34 meV Lorenzian fitted into calculations) and the $\nu=0$ state was found to be about 460 meV (in a diabatic approximation). The vibronic spectra agree with experiment [4,5]. Spin-orbit coupling changes the values marginally but the result is uncertain due to the approximate construction of the diabatic basis. Weak spin-orbit interaction between $^3\Pi_1$ and $^3\Sigma_1^-$ seems to make proper diabatization at long internuclear distances very cumbersome, and we consider the values in Ref. [7] more reliable.

In the adiabatic picture the dissociative $^3\Pi_2$ state becomes weakly bound with a minimum at 1.905 Å on the DHF level and 2.015 Å on the CI level, supporting no vibrational levels.

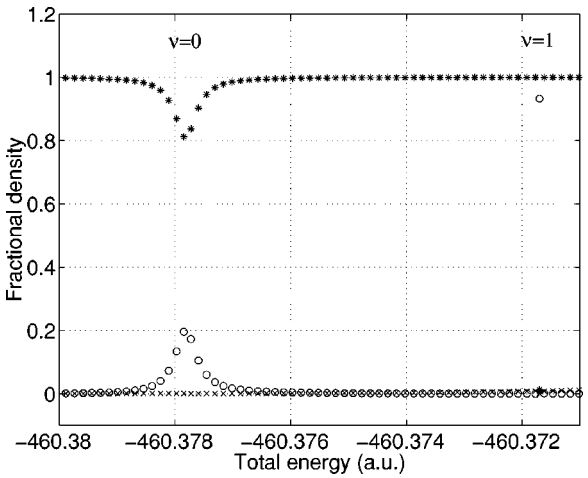

FIG. 3. The density of states in the region of $^1\Sigma_{0-}^+$ – $^3\Pi_{0-}$ crossing. The circles represent the bound state density of $^1\Sigma_{0-}^+$ whereas the crosses and stars represent the continuum state density of $^1\Sigma_{0-}^+$ and $^3\Pi_{0-}$, respectively.

The $^1\Sigma_{0-}^+$ adiabatic potential is found to be repulsive at the DHF level but to have a minimum at the CI level at 1.467 Å with no stable vibrational levels, whereas the dissociative $^3\Pi_{0-}$ becomes weakly bound with a minimum at 1.590 Å at the CI level, supporting one vibrational level. The reduction of vibrational states in the adiabatic approximation, as demonstrated by Banichevich *et al.* [7] as well, is caused by the level crossing which is due to weak spin-orbit interaction. In the region of the crossing the adiabatic approximation fails. Moreover, the crossing is situated in the Franck-Condon region and should thereby have a significant effect on the spectrum. A method based on the full molecular Hamiltonian (rotation neglected) using a diabatic basis must be applied to obtain a correct vibronic profile. In the diabatic picture without spin-orbit interaction the $^1\Sigma_{0-}^+$ possesses two vibrational levels. The bond length is marginally contracted to 1.465 Å. The spin-orbit interaction changes the situation slightly. Figure 3, in which the partial density of bound and different continuum states in variational solution is presented, indicates that the distortion due to spin-orbit interaction is very local: Only the $\nu=0$ state (at about -460.378 a.u.) is significantly affected, whereas the $\nu=1$ state at about -460.372 a.u. remains almost unaffected. Spin-orbit coupling changes the splitting between $\nu=0$ and $\nu=1$ from 163 to 166 meV. In addition, the $\nu=0$ state possesses a small inherent lifetime width of 12 meV due to spin-orbit interaction in agreement with 17 meV obtained by Banichevich *et al.* [7] . Only one level was observed for $^1\Sigma_{0-}^+$ in Refs. [7,5], whereas with AES three levels were observed [4]. Diabatic potential curves and off-diagonal spin-orbit coupling elements are displayed in Fig. 4. We observe a maximum near the crossing point of the diabatic curves of the same order of magnitude as found in [7], but Banichevich *et al.* obtained a much larger change with respect to internuclear distance. The sign of the coupling is taken from Ref. [7].

The CI_v bond lengths are generally 0.03–0.11 Å shorter than the results of Banichevich *et al.* [7]. The $^3\Sigma_{0+}^-$ harmonic constant is in accordance with results of these authors,

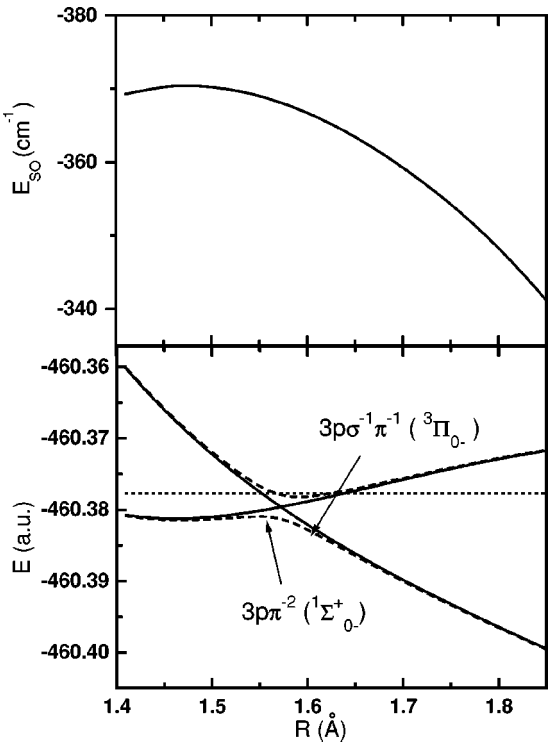

FIG. 4. Off-diagonal spin-orbit coupling elements (E_{SO}) as a function of internuclear distance and CI_v potential-energy curves for the $3p\pi^{-2}$ states $^1\Sigma^+_{0-}$ and $^3\Pi_{0-}$ in the diabatic (solid line) and adiabatic (dashed line) approximations. The dotted line represents the energetic position of the $\nu=0$ state in the diabatic approximation without spin-orbit interaction.

while the anharmonicity constant is 100 cm^{-1} lower on the CI level. Calculated constants are higher than determined in experimental works [5,4].

Adiabatic binding energies are shown in Table IV together with experimental values [5]. The DHF energies are 2.4–2.6 eV lower than their corresponding CI_v energies, which are 0.36–0.47 eV higher than experiment. The MRCI binding energies of Ref. [7], which are in excellent agreement with experiment, were obtained using an experimental, thermodynamic cycle for the ground state to eliminate the basis-set errors and the CI size-consistency error. Although our binding energies are vertically shifted upwards, we find that relative energies deviate only 0.01–0.03 eV from the nonrelativistic results.

III. ENERGIES AND PROFILES OF AUGER TRANSITIONS

A. Kinetic energies

Kinetic energies for Auger electrons were calculated at the CI_v level. Including the vibrational zero-point energies, we found a kinetic energy of 174.16 eV for the $2p^{-1}_{1/2,1/2} \rightarrow 3p\pi^{-2}(^3\Sigma^-_{0+})$ transition. Using single point calculations at the equilibrium distance of the HCl ground state (1.275 Å), we estimate that this value reduces by 60 meV at the CI_{v+c} level. The Gaunt interaction decreases the kinetic energy further by about 0.15–0.20 eV. The experimental kinetic energy for this transition is estimated to be about 173.3 eV [4]. Kinetic energies for other transitions into stable vibrational states can be deduced from Table IV.

B. $2p^{-1}_{j,m_j} \rightarrow 3p\pi^{-2}(^1\Sigma^+_{0-})$, $3p\pi^{-1}\sigma^{-1}$ ($^3\Pi_{0-}$) Auger-electron spectrum

Due to the lack of fully relativistic transition amplitudes, we discuss the simulated AES only for the $2p^{-1}_{j,m_j} \rightarrow 3p\pi^{-2}(^1\Sigma^+_{0-}), 3p\pi^{-1}\sigma^{-1}(^3\Pi_{0-})$ transitions where clear spin-orbit effects are present. The level crossing between $^1\Sigma^+_{0-}$ and $^3\Pi_{0-}$ states, which interact via spin-orbit interaction, is in the Franck-Condon region and thereby changes the spectral features. We want, however, to point out that lifetime vibrational interference plays a significant role for all transitions as observed in [14]. Transitions to vibrational continuum in $3p\pi^{-2}$ states of HCl are also more prominent than in corresponding $4p\pi^{-2}$ states of HBr [3].

The modified form of the interference formula of Correia *et al.* [15] has been used to take into account nonadiabatic effects as in our previous work [3]. The vibronic profile was calculated employing CI_v parameters (diabatic potential curves and off-diagonal spin-orbit coupling elements) and different lifetime widths for core-hole states both from previous calculations by Fink *et al.* [2] and recent experiments [6] for the individual core-hole state. We found that the small variation in equilibrium distances and harmonic constants for $2p^{-1}_{j,m_j}$ states gives rise only to small changes in the AES. The effects of slightly different lifetimes for core holes are also straightforward: The larger width leads to broader peaks and larger lifetime vibrational interference contributions, and vice versa.

The avoided level crossings caused by spin-orbit interaction in the adiabatic approximation was found to lead to local distortion in the vibrational band. However, the small broadenings of stable vibrational states, e.g., of the $\nu=0$ state of $^1\Sigma^+_{0-}$ are very hard to notice from AES due to large lifetime widths of the intermediate core-hole state. We found, however, that the use of the diabatic basis set should be favored in calculations of transition probabilities for the crossing states, if transition amplitudes to both states are comparable. This is very often the case in Auger processes, where the interaction operator (Coulomb operator) rarely leads to strict selection rules. In such cases a small interaction may induce small changes in mixing of states and furthermore in transition amplitudes which may lead to a clear redistribution of intensities. To clarify this, the $2p^{-1}_{1/2,1/2} \rightarrow 3p\pi^{-2}(^1\Sigma^+_{0-})$, $3p\pi^{-1}\sigma^{-1}$ ($^3\Pi_{0-}$) AES is presented in Fig. 5. There are two sharp peaks on the high kinetic energy side and a shoulder around 0.4 eV corresponding to transitions into the stable vibrational states $\nu=0,1$ and a vibrational continuum band of $^1\Sigma^+_{0-}$, respectively. A broad, Gaussian-type band centered at about -1 eV is caused by transitions to dissociative $^3\Pi^+_{0-}$. The effect of spin-orbit interaction is clearly visible and is similar but less prominent than found in HBr^{2+} [3]. (Note, however, that due to an erroneous sign for the spin-orbit coupling element in our previous article, the effects here are opposite with respect to the sign of the transition amplitude.)

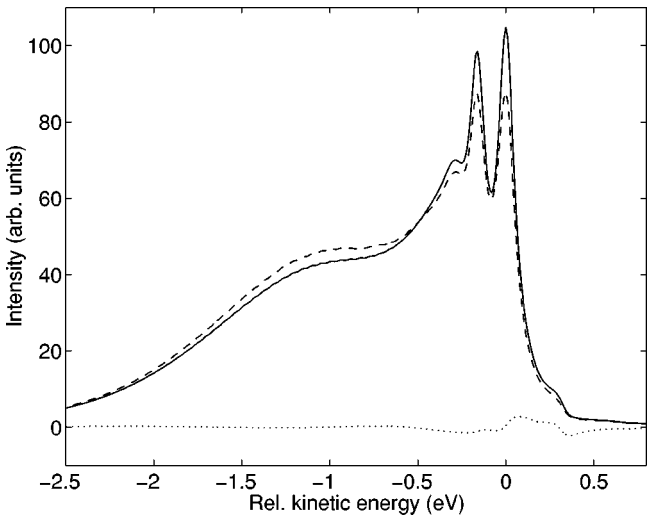

FIG. 5. Calculated vibrational band profile for the $2p^{-1}_{1/2,1/2} \rightarrow 3p\pi^{-2}(^1\Sigma^+_{0-})$, $3p\pi^{-1}\sigma^{-1}$ $(^3\Pi_{0-})$ transition. The dashed line and solid line correspond to the diabatic approximation with and without spin-orbit interactions, respectively. The dotted line is the lifetime vibrational interference contribution with spin-orbit interaction.

IV. CONCLUSIONS

We have presented results from fully relativistic DHF and RASCI calculations on the ground, Cl $2p$−ionized and doubly valence ionized states of HCl. Calculated spectroscopic parameters and binding energies are found to be in correspondence with other calculations and experiment [7,4,5]. Two avoided crossings caused by spin-orbit interaction are observed for the excited states of HCl^{2+}, one of them in the Franck-Condon region leading to changes in the spectral features. A local distortion in the vibrational band by the broadening of 13 meV for the $\nu=0$ vibrational state of $^1\Sigma^+_{0-}$ was observed in good agreement with the value of 17 meV obtained by Banichevich *et al.* [7]. The effect of spin-orbit interaction on the vibronic profile is clearly visible but less prominent than found in HBr^{2+} [3]. Lifetime vibrational interference plays a significant role for all transitions, and transitions to vibrational continuum in $3p\pi^{-2}$ states of HCl are more prominent than in corresponding $4p\pi^{-2}$ states of HBr [3].

A thorough comparison of our results with experiment is still very hard to do. The simultaneous presence of transitions from three $2p^{-1}$ states, the post-collision interaction, or the underlying satellite structure (depending on the photon energy) make the direct comparison of our simulated AES with the experimental AES complicated. The experimental spectra are further complicated by the lifetime vibrational interference and the presence of both stable and continuum vibrational states. However, if recent efforts in the development of the photoelectron Auger-electron coincidence technique [16] turn out to be successful, we can expect real progress in the experimental accuracy. The other source of experimental data, the direct double ionization (see, e.g., [17]), suffers from small cross section and satellite structures. On the theoretical side, our calculations could be improved by an explicit multiconfigurational self-consistent-field study for the individual final states of HCl^{2+}.

ACKNOWLEDGMENTS

This work has received support from The Research Council of Norway (Programme for Supercomputing) through a grant of computing time. Financial support from the Research Council for Natural Sciences of the Academy of Finland is also acknowledged.

[1] K. Ellingsen, T. Saue, H. Aksela, and O. Gropen, Phys. Rev. A **55**, 2743 (1997).
[2] R. Fink, M. Kivilompolo, H. Aksela, and S. Aksela, Phys. Rev. A **58**, 1988 (1998).
[3] T. Matila, K. Ellingsen, T. Saue, H. Aksela, and O. Gropen, Phys. Rev. A **61**, 032712 (2000).
[4] S. Svensson, L. Karlsson, P. Baltzer, M. P. Keane, and B. Wannberg, Phys. Rev. A **40**, 4369 (1989).
[5] A. G. McConkey, G. Dawber, L. Avaldi, M. A. MacDonald, G. C. King, and R. I. Hall, J. Phys. B **27**, 271 (1994).
[6] R. Püttner *et al.* (unpublished).
[7] A. Banichevich, S.D. Peyerimhoff, M.C. Van Hemert, and P.G. Fournier, Chem. Phys. **121**, 351 (1988).
[8] L. Visscher, O. Visser, P.J.C. Aerts, H. Merenga, and W.C. Nieuwpoort, Comput. Phys. Commun. **81**, 120 (1994).
[9] O. Visser, P.J.C. Aerts, D. Hegarty, and W.C. Nieuwpoort, Chem. Phys. Lett. **134**, 34 (1987).
[10] T. H. Dunning, Jr., J. Chem. Phys. **90**, 1007 (1989).
[11] L. Visscher, P.J.C. Aerts, O. Visser, and W.C. Nieuwpoort, Int. J. Quantum Chem., Quantum Chem. Symp. **25**, 131 (1991).
[12] K.P. Huber and G. Herzberg, *Constants of Diatomic Molecules* (Van Nostrand Reinhold, New York, 1979).
[13] L. Visscher, J. Styszyñski, and W.C. Nieuwpoort, J. Chem. Phys. **105**, 1987 (1996).
[14] R. Püttner, Y.F. Hu, G.M. Bancroft, H. Aksela, E. Nõmmiste, J. Karvonen, A. Kivimäki, and S. Aksela, Phys. Rev. A **59**, 4438 (1999).
[15] N. Correia, A. Flores-Riveros, H. Ågren, K. Helenelund, L. Asplund, and U. Gelius, J. Chem. Phys. **83**, 2035 (1985).
[16] M. Neeb, J-E. Rubensson, M. Bierman, and W. Eberhardt, J. Phys. B **29**, 4381 (1996).
[17] L. Avaldi, G. Dawber, N. Gulley, H. Rojas, G. C. King, R. Hall, M. Stuhec, and M. Zitnik, J. Phys. B **30**, 5197 (1997).